NASA TECHNICAL NOTE

NASA TN D-7226

MEASUREMENTS OF SURFACE-PRESSURE FLUCTUATIONS ON THE XB-70 AIRPLANE AT LOCAL MACH NUMBERS UP TO 2.45

by

Thomas L. Lewis

Flight Research Center
Edwards, Calif. 93523

and

Jules B. Dods, Jr., and Richard D. Hanly

Ames Research Center
Moffett Field, Calif. 94035

1. Report No. NASA TN D-7226	2. Government Accession No.	3. Recipient's Catalog No.
4. Title and Subtitle MEASUREMENTS OF SURFACE-PRESSURE FLUCTUATIONS ON THE XB-70 AIRPLANE AT LOCAL MACH NUMBERS UP TO 2.45		5. Report Date March 1973
		6. Performing Organization Code
7. Author(s) Thomas L. Lewis (Flight Research Center), Jules B. Dods, Jr., and Richard D. Hanly (Ames Research Center)		8. Performing Organization Report No. H-714
9. Performing Organization Name and Address NASA Flight Research Center P. O. Box 273 Edwards, California 93523		10. Work Unit No. 501-24-12-00-24
		11. Contract or Grant No.
12. Sponsoring Agency Name and Address National Aeronautics and Space Administration Washington, D. C. 20546		13. Type of Report and Period Covered Technical Note
		14. Sponsoring Agency Code

15. Supplementary Notes

16. Abstract

Measurements of surface-pressure fluctuations were made at two locations on the XB-70 airplane for nine flight-test conditions encompassing a local Mach number range from 0.35 to 2.45. These measurements are presented in the form of estimated power spectral densities, coherence functions, and narrow-band-convection velocities. The estimated power spectral densities compared favorably with wind-tunnel data obtained by other experimenters. The coherence function and convection velocity data supported conclusions by other experimenters that low-frequency surface-pressure fluctuations consist of small-scale turbulence components with low convection velocity.

17. Key Words (Suggested by Author(s)) Aerodynamic noise XB-70 airplane	18. Distribution Statement Unclassified – Unlimited		
19. Security Classif. (of this report) Unclassified	20. Security Classif. (of this page) Unclassified	21. No. of Pages 33	22. Price* $3.00

MEASUREMENTS OF SURFACE-PRESSURE FLUCTUATIONS ON THE

XB-70 AIRPLANE AT LOCAL MACH NUMBERS UP TO 2.45

Thomas L. Lewis
Flight Research Center

and

Jules B. Dods, Jr., and Richard D. Hanly
Ames Research Center

INTRODUCTION

A thorough understanding of environmental conditions is essential when operational commercial air transport vehicles enter high supersonic flight regions. One environmental parameter that has caused concern in recent years is surface-pressure fluctuation. Surface-pressure fluctuations encountered during high-speed flight are of interest primarily because they (1) excite various modes of external vehicle panels and may induce fatigue failures; and (2) radiate into the interior of a vehicle, contributing to passenger irritation and sometimes interfering with the operation of electronic equipment.

Although many experimental studies of surface-pressure fluctuations have been reported in recent years, only a few have included flight-test results, as discussed in references 1 and 2. The most complete flight investigation of the subsonic region was made by Bhat (ref. 1). A limited amount of supersonic data was presented in references 3 and 4.

The present investigation with the XB-70 airplane was designed primarily to obtain in-flight measurements of surface-pressure fluctuations during supersonic cruise conditions. Data were recorded for Mach numbers from 0.35 to 2.45 with two types of transducers. Pressure and force data necessary to compute similarity parameters, which are required for nondimensionalization of the boundary layer, and pressure fluctuations were measured simultaneously at each location with boundary-layer rakes and skin-friction gages. Measurements were made at two different locations on the airplane. A microphone array was used at one location and a single microphone at the other. Data from the array are presented in this report in terms of estimated power spectral density, coherence function, and convection velocities. Data from the single microphone are presented in terms of estimated power spectral densities.

Because of the general similarity of the turbulent boundary-layer surface-pressure-fluctuation fields, data of this study are compared with wind-tunnel-wall data from reference 5 and wind-tunnel and flight data from reference 2.

SYMBOLS

Physical quantities in this report are given in the International System of Units (SI) and parenthetically in U.S. Customary Units. Calculations and measurements were made in Customary Units. Factors relating the two systems are presented in reference 6.

C_f local skin-friction coefficient

f frequency, Hz

h_p pressure altitude, m (ft)

M local Mach number

$\hat{P}'$ nondimensional power spectral density, $\log_{10}\left[\dfrac{P^2(\omega)U}{2\delta^*} \times 10^3\right]$

$\sqrt{\overline{P^2}}$ root-mean-square value of surface-pressure fluctuations, hN/m^2 (lb/ft^2)

$\overline{P^2}(\omega)$ estimated power spectral density as a function of circular frequency, $(hN/m^2)^2 sec$ $((lb/ft^2)^2 sec)$

q local dynamic pressure, hN/m^2 (lb/ft^2)

R Reynolds number per unit length, m^{-1} (ft^{-1})

T_t total temperature, °K (°R)

U local velocity, m/sec (ft/sec)

U_c narrow-band-convection velocity, m/sec (ft/sec)

α angle of attack, deg

$\gamma^2(\psi)$ coherence function (ref. 7)

δ^* boundary-layer-displacement thickness, m (ft)

Θ boundary-layer-momentum thickness, m (ft)

Θ' phase angle, rad

Λ nondimensional frequency, $\log_{10}\left(\dfrac{\omega\delta^*}{U} \times 10^4\right)$ (ref. 2)

ξ separation distance between transducers, m (ft) or cm (in.)

2

τ_ω skin friction, hN/m^2 (lb/ft^2)

ψ nondimensional frequency, $\log_{10}\left(\dfrac{f\xi}{U} \times 10^3\right)$

ω circular frequency, $2\pi f$, rad/sec

Subscript:

∞ free stream

EQUIPMENT AND INSTRUMENTATION

XB-70 Airplane

The XB-70 airplane, designed for Mach 3 cruise flight, was used as the test-bed for this study. A photograph of the airplane is shown in figure 1, and a three-view drawing, with dimensions, is shown in figure 2. The design gross weight of the airplane is in excess of 227,000 kilograms (500,000 pounds). It has a thin, low-aspect-ratio, highly swept delta wing (65.6°) with downward folding wing tips, twin movable vertical stabilizers, elevon surfaces for pitch and roll control, a movable canard with trailing-edge flaps, and twin inlets integrated into a propulsion nacelle beneath the wing. Propulsion is provided by six YJ93-GE-3 engines each with a thrust of approximately 133,000 newtons (30,000 pounds) for standard sea-level conditions. A more detailed description of the airplane is included in reference 8.

Surface-Pressure-Fluctuation Transducers

Two types of transducers, Kulite and Photocon, were used to measure the surface-pressure fluctuations. Pertinent details about the transducers are presented in table 1. A detailed description of the calibration and the experimental results obtained with these transducers are presented in reference 5.

Instrumentation Locations

Two locations on the XB-70 airplane were chosen for surface-pressure-fluctuation measurements: the fuselage centerline on the lower surface under the cockpit; and the upper surface of the right wing a short distance forward of the vertical stabilizer. The approximate positions of these measurement locations are indicated in figure 2. These locations were selected because of the relatively undisturbed, clean flow conditions in the areas and the availability for use.

Photographs of the instrumentation at location 1 are shown in figure 3. The Preston probe and boundary-layer rake were used to obtain local boundary-layer-flow measurements. The skin-friction gage was used primarily in another program. The rake, probe, and gage are described in reference 9. A sketch of the transducer arrays

is presented in figures 4(a) and 4(b). The transducers were positioned to obtain a logarithmic displacement in order to minimize the number of transducers necessary to adequately define the surface-pressure-fluctuation field.

A fence to induce boundary-layer separation was installed at location 1 so that measurements could be made in a region of separated flow. Photographs of the modified installation are presented in figure 5. The fence, which was positioned approximately 0.051 meter (0.19 foot) behind transducer location P8 (fig. 4(b)), was 0.05 meter (0.17 foot) high, 0.30 meter (1 foot) wide, and 0.002 meter (0.08 foot) thick.

The boundary-layer instrumentation at location 2 was similar to that at location 1 (ref. 9) except that only one surface-pressure-fluctuation transducer was used. Photographs of the installation are shown in figure 6.

DATA ACQUISITION AND REDUCTION

The surface-pressure-fluctuation data were recorded onboard the airplane on an analog tape recorder. A tape speed of 1.52 meters (60 inches) per second and frequency-modulated record amplifiers provided a frequency response of 0 to 20,000 cycles per second and a dynamic range of 50 decibels. A single-stack, 14-channel IRIG standard recording head was used to minimize skew. (Cross-power spectral density analysis is simplified if skew or phase between tracks is minimized.)

The data from location 1 were reduced at the NASA Ames Research Center with a hybrid analog-digital computer system (ref. 10). The statistical accuracy of the system varied with frequency, as indicated by the normalized standard errors presented in terms of percentage in table 2 (adapted from ref. 11). Normalized standard error is defined as the $\dfrac{\text{Variance of sample mean value}}{\text{True mean square value}} \times 100$. According to reference 7, the normalized standard error can be determined by using the following formula: $\dfrac{1}{(\text{Filter bandwidth})(\text{Averaging time})}$. Power spectral densities, coherence functions, narrow-band-convection velocities, and overall pressure-fluctuation levels were obtained by using this analysis system.

Estimated power spectral densities of the surface-pressure fluctuations from location 2 were determined by using a Federal Scientific UA-6 spectrum analyzer with a range of 0 to 20,000 hertz. With this analyzer, 500 40-cycle wide bandpass filters and ensemble averaging of 64 samples were used to obtain 128 degrees of freedom. The estimated power spectral density data are presented as smooth curves which represent fairings of the analyzed results. These power spectral density data were reduced at the NASA Flight Research Center.

Boundary-layer-flow data were recorded on magnetic tape and were reduced to local boundary-layer-momentum thickness, Θ, boundary-layer-displacement thickness, δ^*, Mach number, M, velocity, U, dynamic pressure, q, and skin-friction coefficient, C_f, using methods outlined in reference 9. Additional boundary-layer data are presented in reference 9. Stagnation temperature was assumed to be constant, and static pressure was assumed to be constant throughout the boundary layer.

4

FLIGHT-TEST CONDITIONS

The pilot maintained steady-state flight-test conditions by monitoring velocity and altitude. When these parameters remained invariant to within approximately 5 percent, data were recorded for 30 seconds. The flight-test conditions encompassed velocities from 118 to 696 meters per second (386 to 2285 feet per second), altitudes from 888 to 19,000 meters (2910 to 62,400 feet), and corresponding Mach numbers from 0.35 to 2.45. The data in this report were obtained during two flights.

RESULTS AND DISCUSSION

Values of the flow parameters used in this analysis are given in tables 3 and 4 for each flight-test condition.

Power Spectral Densities

Nondimensionalized power spectral density data obtained from the Kulite transducers at location 1 for all the flight-test conditions are presented in figure 7. The key includes a schematic drawing of the transducer array. Except for the data from transducer K3 at $M = 0.60$, there are no clear indications that a maximum value of the power spectral density has been determined. This was not unexpected; similar results were obtained with a Photocon transducer in the study of reference 5.

Experience with Kulite transducers (ref. 5) indicated that, in general, any differences in power spectral densities in the Kulite transducer data were related predominantly to the nature of the surface-pressure-fluctuation field rather than to a surface interaction effect caused by the presence of the transducers.

Nondimensionalized power spectral density data obtained from the Photocon transducers at location 1 are presented in figure 8. Data are shown for only three of the flight-test conditions. At Mach numbers above 1.1, the transducer system malfunctioned. Although the cause of the malfunction was not established conclusively, it may have been related to the temperature—altitude environment and the Photocon preamplifier. Attempts to duplicate the failure in laboratory tests were unsuccessful.

There does not seem to be a clear explanation of the differences in the power spectral density data obtained from the three Photocon transducers for any one test condition. Even though the surface flushness of each transducer was held to 0.000 and -0.00254 centimeter (0.000 and -0.001 inch), a surface interaction effect might have contributed to the discrepancies. (See references 1 and 5.)

Data obtained from the Photocon transducer at location 2 are presented in figure 9. The data for $M = 0.66$ in figure 9(a) are believed to have been affected by engine noise. The first harmonic peak corresponds to the fundamental frequency produced by the first stage of the engine compressor. The absence of engine noise at the lower Mach numbers was not explained definitively, but it may have been caused by a change in the

5

propagation path of the sound. The supersonic data from location 1 (fig. 8) are similar to the supersonic data from location 2 in figures 9(a) to 9(c). The frequency analysis range for these data was limited at the lowest frequencies because of the lower limit of analysis of the Federal Scientific UA-6 spectrum analyzer.

The nondimensionalized power spectral density data obtained at location 1 from the Kulite transducers are presented in figure 10 and from the Photocon transducers in figure 11. These data are compared with results of other experimenters compiled by Bies (ref. 2) and wind-tunnel data from reference 5.

The data obtained with the Kulite transducers (fig. 10) agree with the power spectral density prediction of reference 2 and the wind-tunnel data of reference 5. It should be noted that the reference 5 wind-tunnel tests were for supersonic Mach numbers only.

The data from the Photocon transducers (fig. 11) show good agreement with the reference 2 power spectral density prediction for supersonic Mach numbers and with the wind-tunnel data of reference 5. The subsonic data obtained from the Photocon transducers are somewhat lower than the prediction.

The location 2 data presented in figure 12 were obtained for several Mach numbers with one Photocon transducer. The results appear to be higher than the wind-tunnel data summarized by Bies in reference 2. This is not unexpected; other flight data summarized by Bies have also been higher. Bies indicated that this difference in the data could have been caused by surface roughness and protuberances over the surface flow length. Similar effects are believed to be responsible in this instance.

Coherence Functions

A coherence function is used to obtain a measure of the decay of a surface-pressure fluctuation as it travels downstream. The coherence function between any two transducers is determined by obtaining the square of the absolute magnitude of the cross-spectral density and dividing this value by the product of the power spectral densities from each transducer. (See page 103 of reference 7.) When the coherence function equals zero at a particular frequency, the surface-pressure fluctuation measured by each transducer is said to be unrelated. This implies that the surface-pressure fluctuation at that frequency has decayed beyond recognition while traveling between transducers.

Coherence functions were determined for three separation distances between Kulite transducers at location 1. These data are shown in figure 13. Over a Mach number range from 0.35 to 1.62 (figs. 13(a) to 13(d)), the coherence function presented as ξ/δ^* becomes zero at some nondimensional frequency above 3. Just prior to the decrease of the coherence function to zero, there is a peak at the mid-nondimensional frequencies. The nondimensional frequency at which this peak value occurs increases with increasing Mach number. The maximum value of the coherence function generally decreases with an increase in the magnitude of transducer separation distance divided by boundary-layer thickness. The maximum value of the coherence function for the largest transducer separation distance occurs at the lowest nondimensional frequency shown. The coherence function for the largest transducer separation distance has what

6

might be termed a secondary maximum at a higher nondimensional frequency, similar to the peak coherence function for the smaller separation distances. Because the value of the coherence function should be greatest for a nondimensional frequency near zero, the coherence function for the smallest transducer separation distances would be larger if lower frequency data were available.

For the Mach 1.92 data (fig. 13(e)) the coherence function level is high for the two smallest separation distances over a large frequency range. This relatively high overall level may be related to the fact that the angle of attack for these data was lower than for any other data presented. A detailed discussion of the variation of boundary-layer parameters with flight conditions at this location on the XB-70 airplane is presented in reference 9.

The coherence functions for the Mach 1.92 (fig. 13(e)), 2.11 (fig. 13(g)), and 2.21 (fig. 13(h)) data are similar to the coherence functions for Mach numbers below 1.92. The coherence functions for all separation distances for all Mach numbers except 2.24 converge at the higher nondimensional frequencies. The reason for this exception is not known.

Narrow-Band-Convection Velocity

A narrow-band-convection velocity represents a series of pressure fluctuations in a flow passing two or more positions at some frequency. Convection velocity is defined by the equation:

$$U_c = \xi\omega/\Theta'$$

where Θ' is determined by $\tan^{-1}$ (cospectral density divided by quadspectral density, ref. 7).

Data taken at the nine flight-test conditions over three transducer separation distances are presented in figure 14. The data appear to be similar. In general, the lowest frequencies were convected at the lowest speeds, and a small band of intermediate frequencies was convected at speeds approaching the local free-stream velocity. Convection velocity decreased at the higher frequencies. Although there was some scatter in the data at the lower frequencies, the trends were evident, as shown by the curves. These data agree with Bull's theoretical discussions of surface-pressure fluctuation presented by Richards in reference 12: principally, that small-scale turbulence is convected slowly, appearing as low-frequency surface-pressure fluctuations to the transducer.

Blake showed in reference 13 that very low convection velocities existed at low frequencies and that convection velocity increased with increasing frequencies, reached a maximum, and then converged to an intermediate value. The data from reference 13 and the present data are compared in figure 15. The agreement is considered to be good. Although Blake's data ($M \approx 0.16$) showed that the narrow-band-convection velocities for small separation distances decreased sharply with decreasing frequency and that there was considerably less frequency dependence with increasing separation distances between transducers, the data of the present study indicate the same low-frequency trends for all separation distances. This seeming discrepancy may be a function of the limited amount of data available to Blake.

Chyu and Hanly (ref. 11) also presented narrow-band-convection velocity data for a pressure-fluctuation field on a body of revolution in a wind tunnel for a Mach number of 2. Fairings of these data are compared in figure 16 with data from the present study having similar values of ξ/δ^*. Again, the data are similar; however, Chyu and Hanly showed only the high-frequency trends. They also concluded that the narrow-band-convection velocity would converge to free-stream velocity in the lowest frequencies.

Separated Flow

The effect of a separated region of the surface flow on the pressure-fluctuation field is illustrated in figure 17. The relative maximums in the variation of $\sqrt{\overline{P^2}/q}$ indicate the location of the shock buildup caused by the separated region; the lowest values of $\sqrt{\overline{P^2}/q}$ to the left of these peaks indicate the unseparated flow region. The largest levels of $\sqrt{\overline{P^2}/q}$ are in the region of separation. The fairings of the data obtained behind the boundary-layer-separation-inducing fence are based on unpublished data obtained by Chyu and Hanly.

CONCLUDING REMARKS

Measurements of surface-pressure fluctuations for nine flight-test conditions encompassing a local Mach number range from 0.35 to 2.45 were made at two locations on the XB-70 airplane. These measurements were presented in the form of nondimensionalized power spectral densities, coherence functions, and convection velocities.

The nondimensionalized power spectral densities compared favorably with wind-tunnel data obtained by other experimenters.

The coherence function and convection velocity data supported conclusions by other experimenters that low-frequency surface-pressure fluctuations are small-scale turbulence components convected at less than free-stream velocity and therefore sensed by the transducer as long-wavelength pressure fluctuations.

Flight Research Center,
  National Aeronautics and Space Administration,
    Edwards, Calif., November 13, 1972.

REFERENCES

1. Bhat, W. V.: Flight Test Measurement of Exterior Turbulent Boundary Layer Pressure Fluctuations on Boeing Model 737 Airplane. J. Sound and Vibration, vol. 14, no. 4, Feb. 1971, pp. 439-457.

2. Bies, D. A.: A Review of Flight and Wind Tunnel Measurements of Boundary Layer Pressure Fluctuations and Induced Structural Response. Bolt Beranek and Newman Inc. (NASA CR-626), 1966.

3. Belcher, Peter M.: Predictions of Boundary-Layer-Turbulence Spectra and Correlations for Supersonic Flight. Reports of the Fifth International Congress on Acoustics, vol. Ib, 1965, pp. L54 (1-4).

4. McLeod, Norman J.: Flight-Determined Aerodynamic-Noise Environment of an Airplane Nose Cone Up to a Mach Number of 2. NASA TN D-1160, 1962.

5. Lewis, Thomas L.; and Dods, Jules B., Jr.: Wind-Tunnel Measurements of Surface-Pressure Fluctuations at Mach Numbers of 1.6, 2.0, and 2.5 Using 12 Different Transducers. NASA TN D-7087, 1972.

6. Mechtly, E. A.: The International System of Units - Physical Constants and Conversion Factors. NASA SP-7012, 1969.

7. Bendat, Julius S.; and Piersol, Allan G.: Measurement and Analysis of Random Data. John Wiley & Sons, Inc., c.1966, p. 186.

8. Andrews, William H.: Summary of Preliminary Data Derived from the XB-70 Airplanes. NASA TM X-1240, 1966.

9. Fisher, David F.; and Saltzman, Edwin J.: Local Skin Friction Coefficients and Boundary-Layer Profiles Obtained in Flight From the XB-70-1 Airplane at Mach Numbers Up to 2.5. NASA TN D-7220, 1973.

10. Lim, R. S.; and Cameron, W. D.: Power and Cross-Power Spectrum Analysis by Hybrid Computers. NASA TM X-1324, 1966.

11. Chyu, W. J.; and Hanly, R. D.: Power- and Cross-Spectra and Space-Time Correlations of Surface Fluctuating Pressures at Mach Numbers Between 1.6 and 2.5. NASA TN D-5440, 1969.

12. Richards, E. J.; and Mead, D. J.: Noise and Acoustic Fatigue in Aeronautics. Ch. 8, M. K. Bull, John Wiley & Sons, Ltd., 1968, p. 179.

13. Blake, W. K.: Turbulent Boundary-Layer Wall-Pressure Fluctuations on Smooth and Rough Walls. Fluid Mech., vol. 44, part 4, Dec. 1970, pp. 637-660.

TABLE 1. – TRANSDUCER INFORMATION

Transducer	Type	Sensitivity, dB	Estimated sensitive diameter, cm (in.)	Manufacturer
Kulite	Diffusion bonded, semiconductor, strain-gage, pressure transducer model XPL-125-4HF	-63	0.102 (0.04)	Kulite Semiconductor Products, Inc.
Photocon	Condenser microphone model 734	-50	0.305 (0.12)	Whittaker Corp.

10

TABLE 2. – OPERATING PARAMETERS USED IN THE HYBRID ANALOG–DIGITAL

ANALYSIS OF POWER SPECTRAL DENSITIES

Frequency range, Hz	Filter bandwidth, cycles	Averaging time, sec	Number of filters	Normalized standard error of power spectral densities, percent
10 to 50	2	20	21	15.8
60 to 240	10	20	19	7.0
260 to 1,020	40	10	20	5.0
1,200 to 5,200	200	2	21	5.0
5,600 to 10,400	400	2	13	3.5
11,200 to 20,000	800	2	12	2.5

11

TABLE 3. - FLOW PARAMETERS FOR TEST DATA (LOCATION 1)

	M								
	0.35	0.60	1.10	1.62	1.92	1.95	2.11	2.21	2.24
U_∞, m/sec (ft/sec)	118 (386)	187 (612)	329 (1080)	478 (1568)	575 (1887)	591 (1938)	645 (2117)	674 (2210)	693 (2273)
q_∞, hN/m² (lbf/ft²)	.81 (163)	1.01 (202)	1.54 (310)	2.15 (431)	3.31 (664)	1.91 (382)	2.92 (586)	2.42 (485)	2.33 (468)
R, m⁻¹ (ft⁻¹)	7.58×10^6 (2.31×10^6)	6.76×10^6 (2.06×10^6)	6.07×10^6 (1.85×10^6)	6.04×10^6 (1.84×10^6)	7.55×10^6 (2.3×10^6)	4.17×10^6 (1.27×10^6)	5.77×10^6 (1.76×10^6)	4.56×10^6 (1.39×10^6)	4.20×10^6 (1.28×10^6)
δ^*, m (ft)	.0059 (.0192)	.0068 (.0222)	.0085 (.028)	.0108 (.0355)	.0152 (.05)	.0283 (.093)	.0229 (.075)	.0202 (.0664)	.0171 (.056)
Θ, m (ft)	.0041 (.0133)	.0045 (.0147)	.0044 (.0144)	.0044 (.0144)	.0053 (.0173)	.0096 (.0314)	.0071 (.0234)	.0061 (.0201)	.0050 (.0164)
C_f	2.05×10^3	2.13×10^3	2.01×10^3	1.97×10^3	1.63×10^3	2.02×10^3	2.01×10^3	2.02×10^3	2.02×10^3
h_p, m (ft)	$.888 \times 10^3$ (2.91×10^3)	7.56×10^3 (24.79×10^3)	12.8×10^3 (42.08×10^3)	15.4×10^3 (50.6×10^3)	14.9×10^3 (48.7×10^3)	18.5×10^3 (60.9×10^3)	16.9×10^3 (55.3×10^3)	18.6×10^3 (61.0×10^3)	19.0×10^3 (62.4×10^3)
T_t, °K (°R)	286 (517)	255 (459)	275 (495)	331 (596)	388 (699)	402 (725)	439 (791)	458 (825)	477 (860)
α, deg	6.5	6.5	5.6	6.0	3.7	4.9	4.3	4.5	4.6

12

TABLE 4.– FLOW PARAMETERS FOR TEST DATA (LOCATION 2)

	M								
	0.40	0.66	1.10	1.65	1.94	2.12	2.28	2.34	2.45
U_∞, m/sec (ft/sec)	130 (427)	203 (667)	319 (1046)	484 (1588)	578 (1895)	661 (2170)	671 (2203)	682 (2238)	696 (2285)
q_∞, hN/m² (lbf/ft²)	.981 (197)	1.15 (230)	1.66 (333)	2.14 (430)	3.45 (693)	2.04 (409)	3.15 (632)	2.44 (489)	2.46 (494)
R, m⁻¹ (ft⁻¹)	8.27×10^6 (2.52×10^6)	7.09×10^6 (2.16×10^6)	7.02×10^6 (2.14×10^6)	5.84×10^6 (1.78×10^6)	7.91×10^6 (2.41×10^6)	3.81×10^6 (1.16×10^6)	6.36×10^6 (1.94×10^6)	4.92×10^6 (1.50×10^6)	5.09×10^6 (1.55×10^6)
δ^*, m (ft)	.0158 (.0517)	.0239 (.0785)	.0209 (.0687)	.0317 (.1039)	.0394 (.130)	.0513 (.1682)	.0343 (.113)	.0589 (.193)	.067 (.220)
Θ, m (ft)	.0094 (.0310)	.0144 (.0474)	.00967 (.0317)	.0116 (.0380)	.0125 (.0412)	.0148 (.0486)	.0092 (.0301)	.0153 (.0501)	.0165 (.054)
C_f	1.91×10^3	1.74×10^3	1.21×10^3	1.30×10^3	1.30×10^3	1.21×10^3	1.54×10^3	1.27×10^3	1.18×10^3
h_p, m (ft)	$.888 \times 10^3$ (2.91×10^3)	7.56×10^3 (24.79×10^3)	12.8×10^3 (42.08×10^3)	15.4×10^3 (50.6×10^3)	14.9×10^3 (48.7×10^3)	18.5×10^3 (60.9×10^3)	16.9×10^3 (55.3×10^3)	18.6×10^3 (61.0×10^3)	19.0×10^3 (62.4×10^3)
T_t, °K (°R)	287 (518)	255 (459)	256 (462)	330 (595)	387 (696)	459 (827)	439 (791)	442 (797)	442 (797)
α, deg	6.5	6.5	5.6	6.0	3.7	4.9	4.3	4.5	4.6
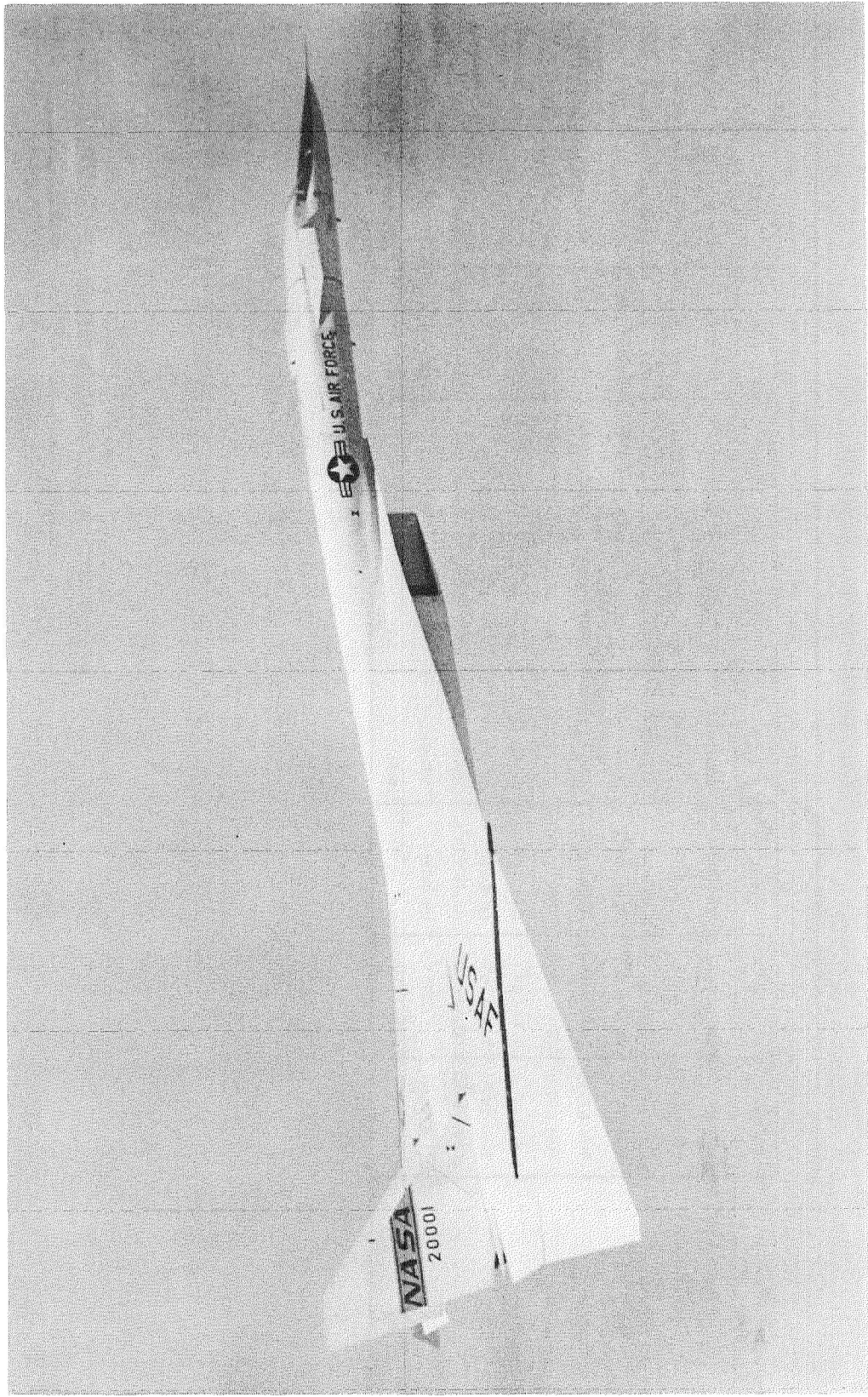
Figure 1. Photograph of the XB-70 in flight.

E-17463
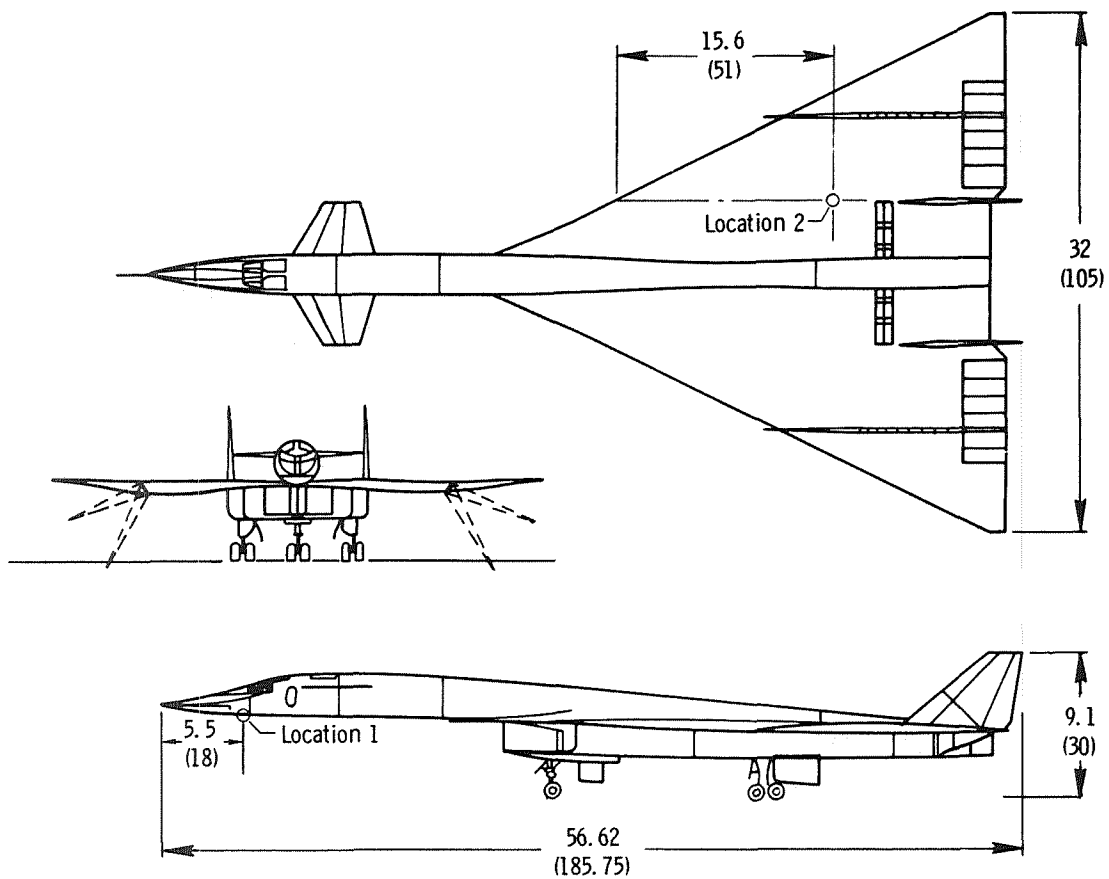
Figure 2. Three-view drawing of the XB-70 airplane showing locations used for surface-pressure-fluctuation measurements. Dimensions are in meters (feet).
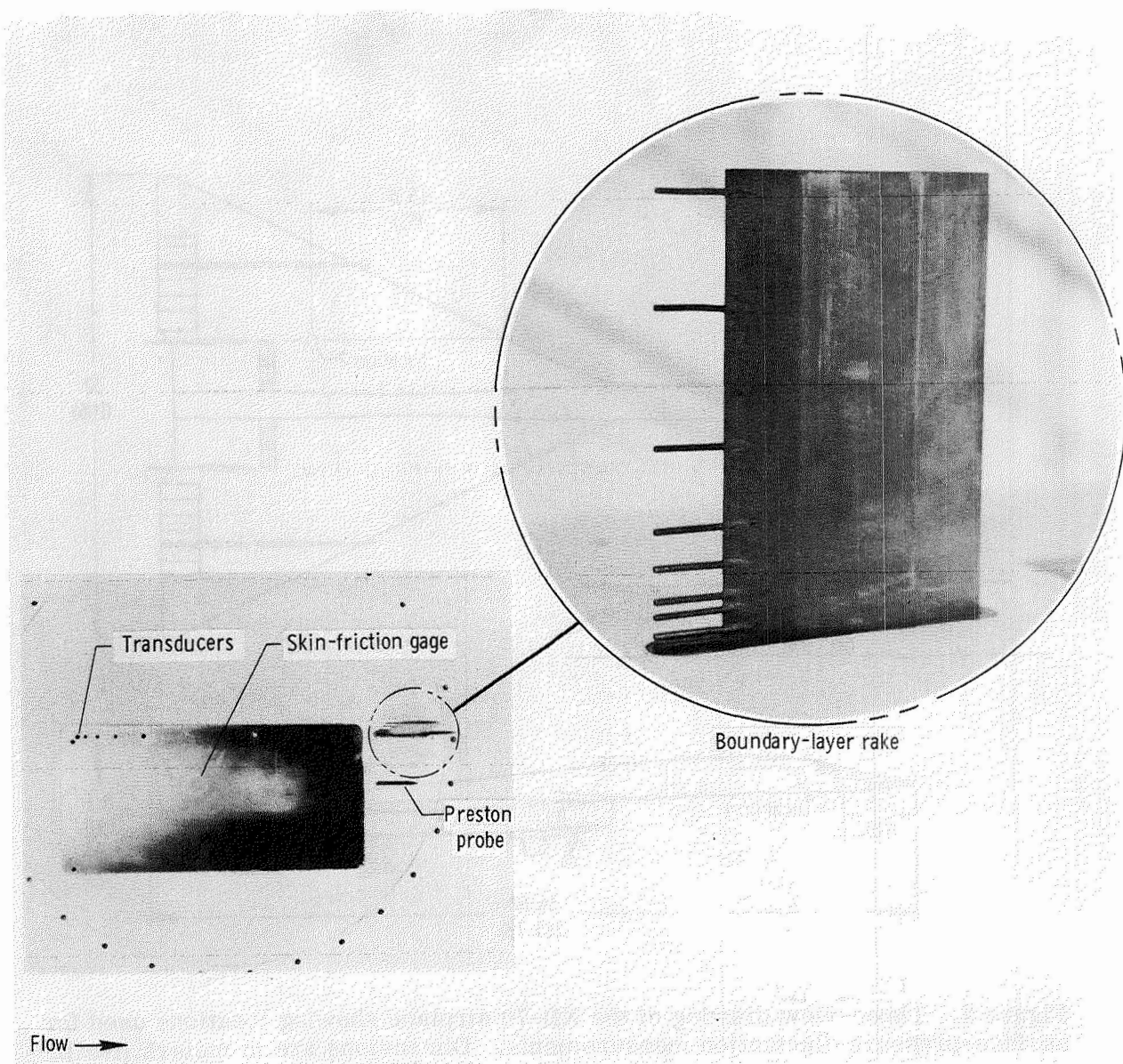
Figure 3. Photographs of the instrumentation at location 1.
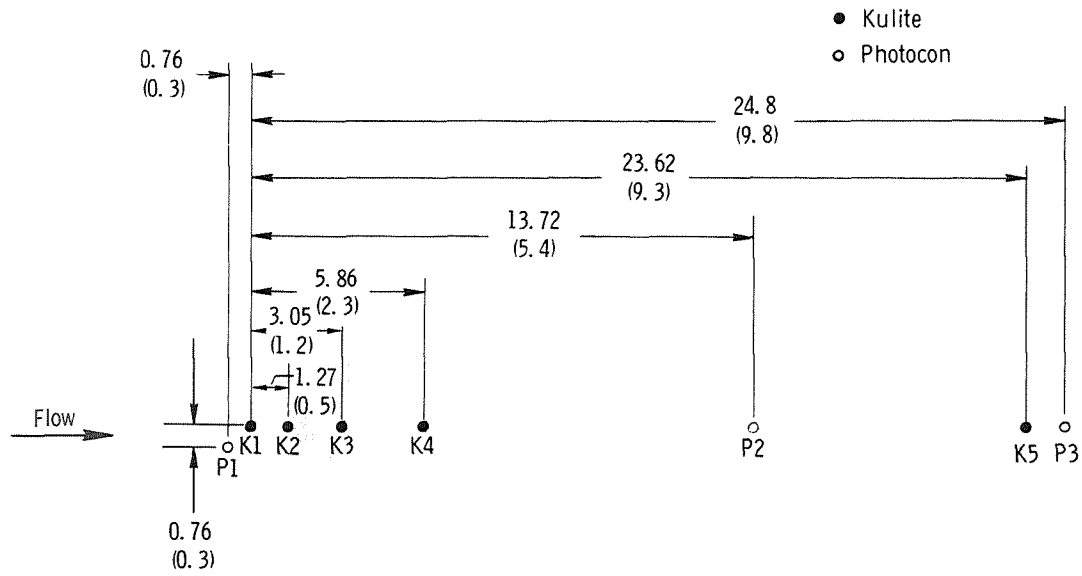
(a) Instrumentation for normal flow.
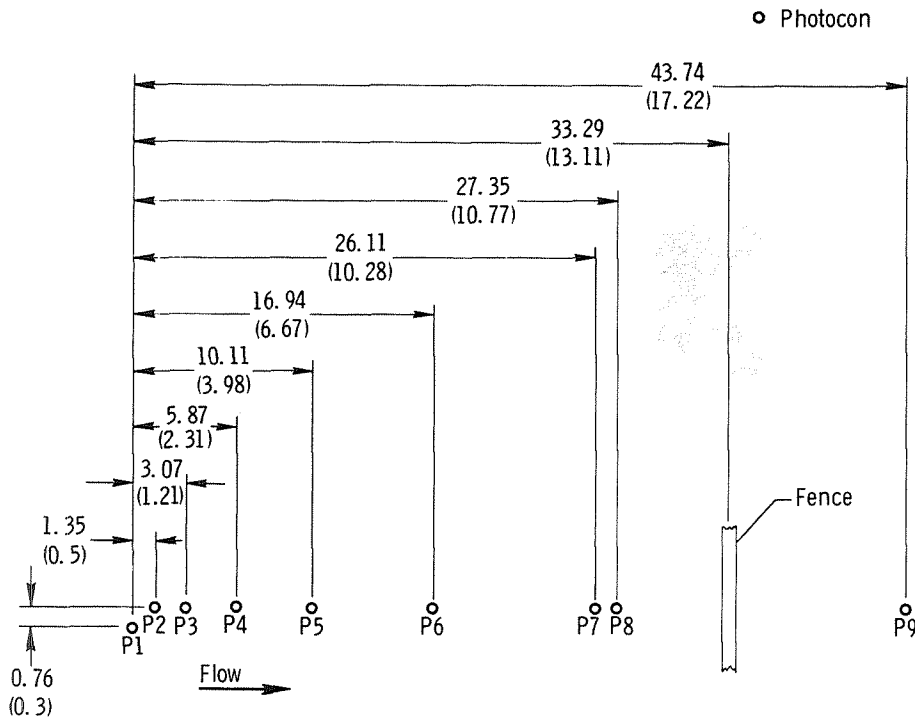
(b) Instrumentation for separated flow.

Figure 4. Sketch showing the transducer positions in the arrays at location 1. Location designations are indicated below each transducer; dimensions are in centimeters (inches).
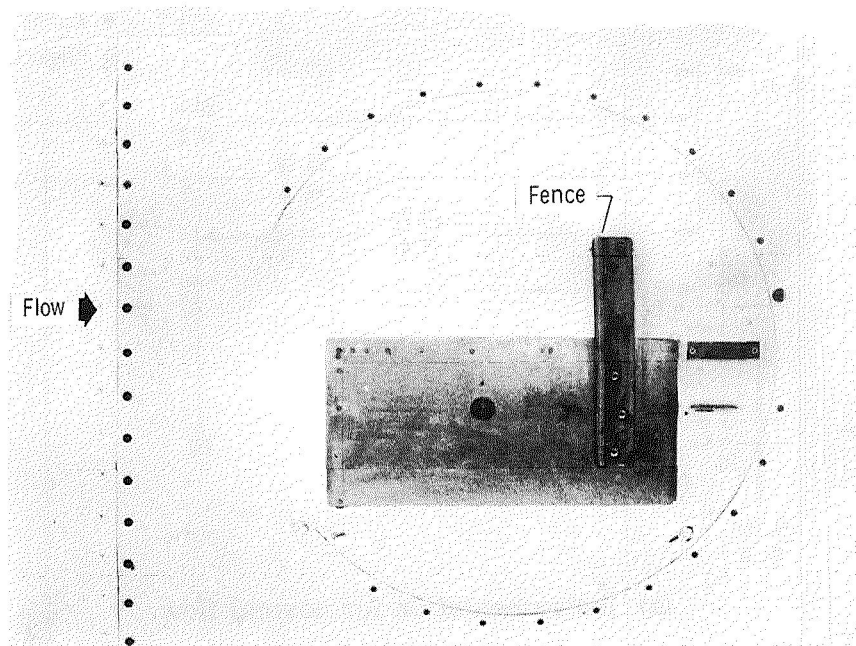
(a) Plan view.
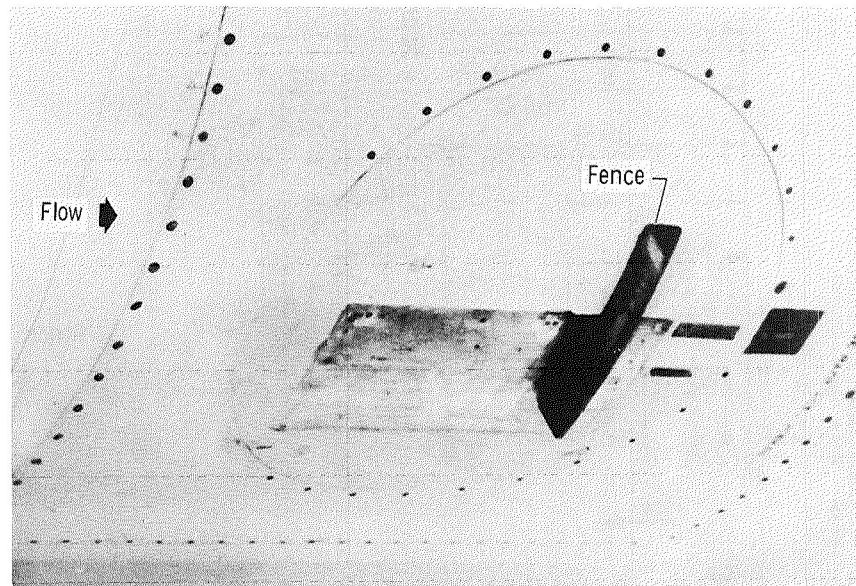
(b) Perspective view.

Figure 5. Photographs of location 1 showing the boundary-layer-separation-inducing fence.

18
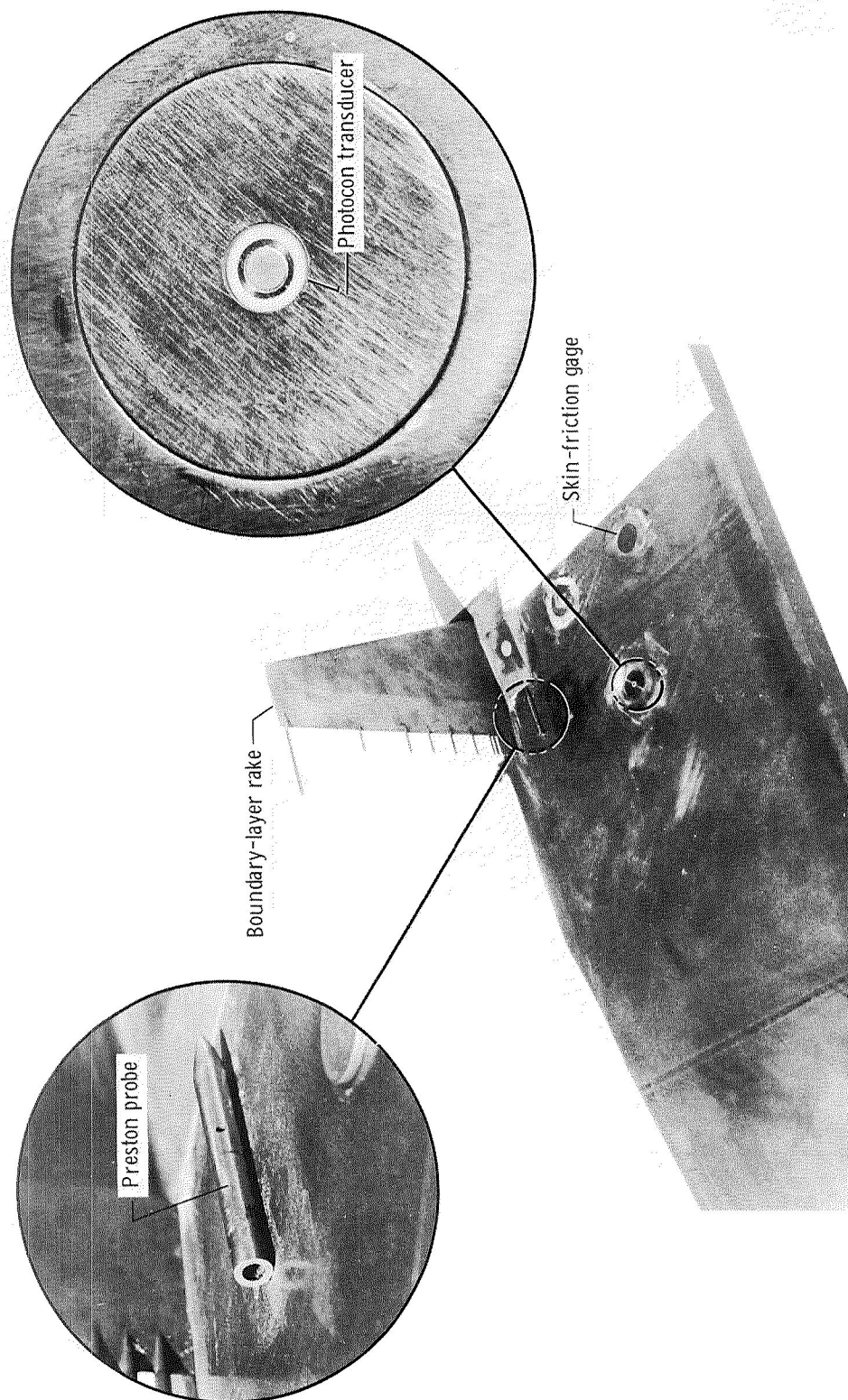
Figure 6. Photographs of the instrumentation at location 2.
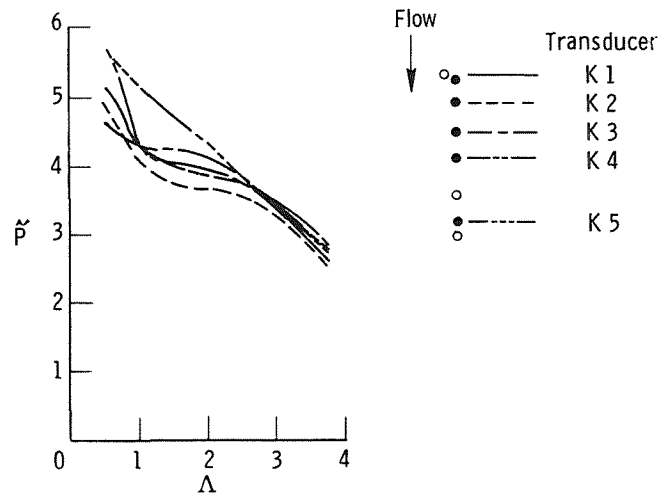
(a) M = 0.35.
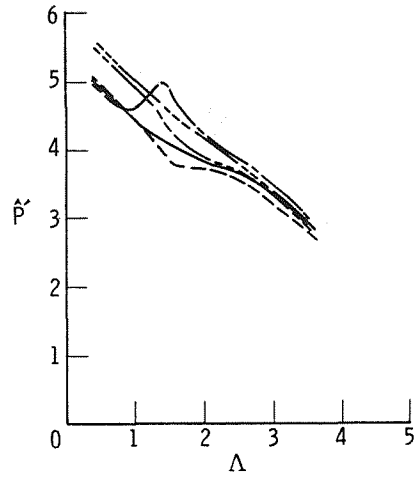
(b) M = 0.60.
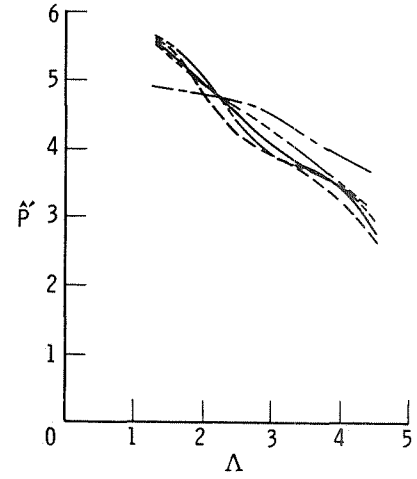
(c) M = 1.10.

Figure 7. Nondimensionalized power spectral density data obtained from the Kulite transducers at location 1.
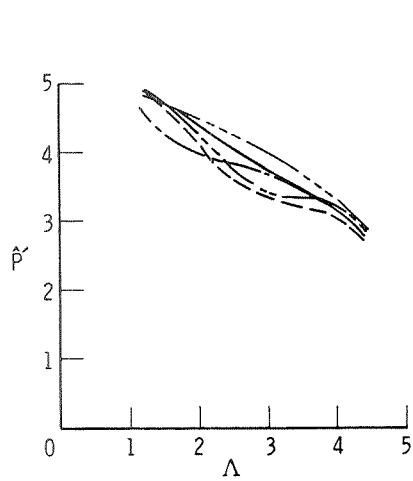
(d) M = 1.62.
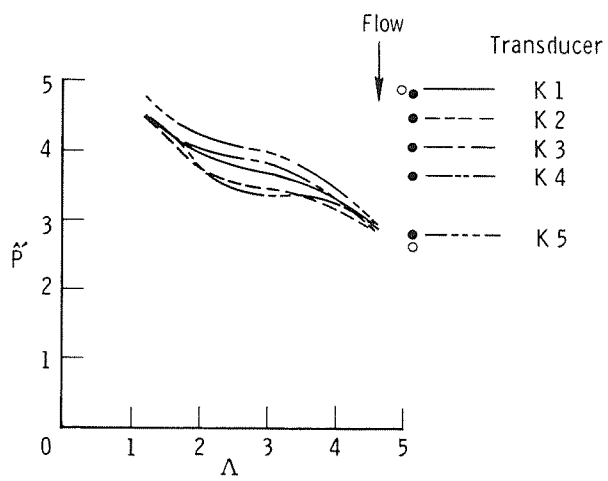
(e) M = 1.92.
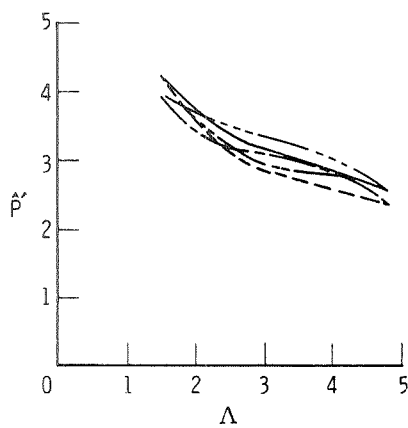
(f) M = 1.95.
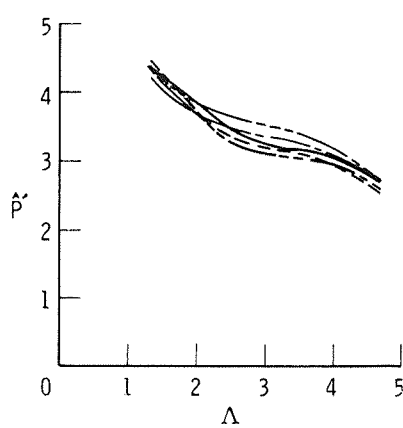
(g) M = 2.11.
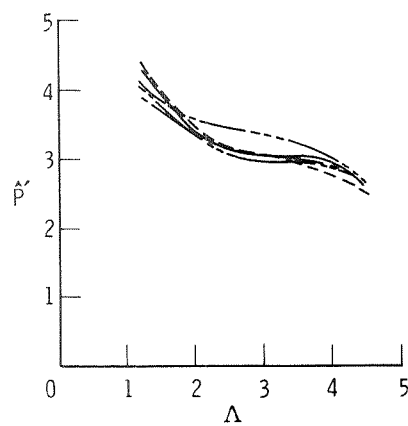
(h) M = 2.21.
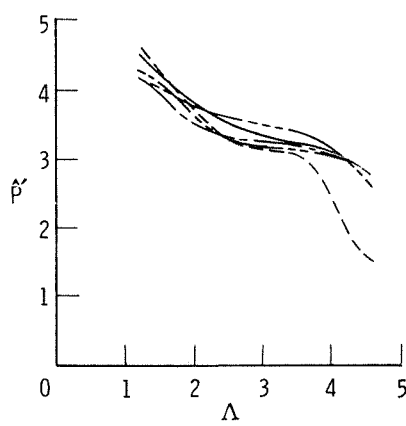
(i) M = 2.24.

Figure 7. Concluded.
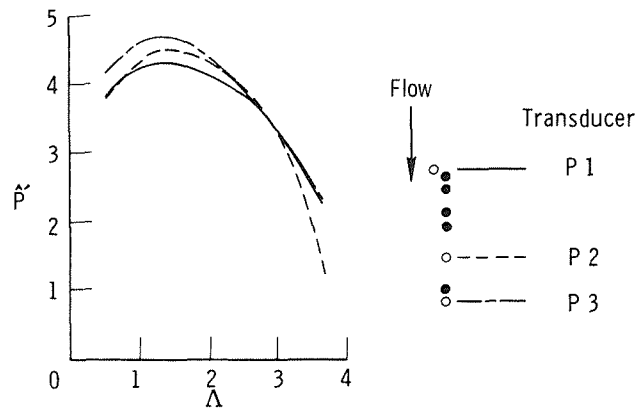
(a) M = 0.35.
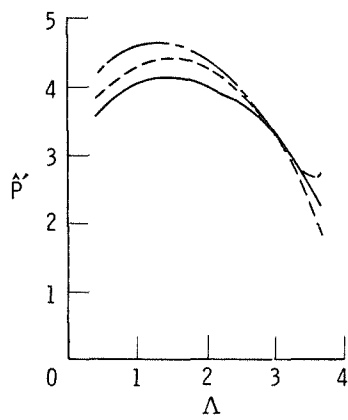
(b) M = 0.60.
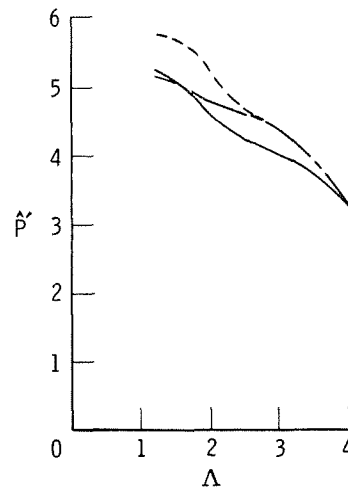
(c) M = 1.10.

Figure 8. Nondimensionalized power spectral density data obtained from the
Photocon transducers at location 1.
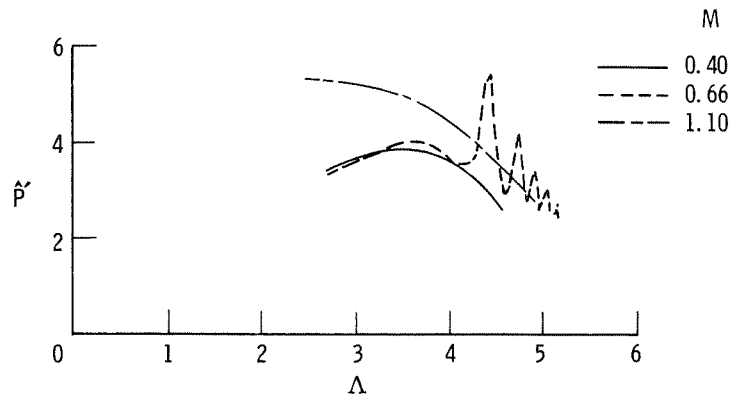
(a) M = 0.40 to 1.10.
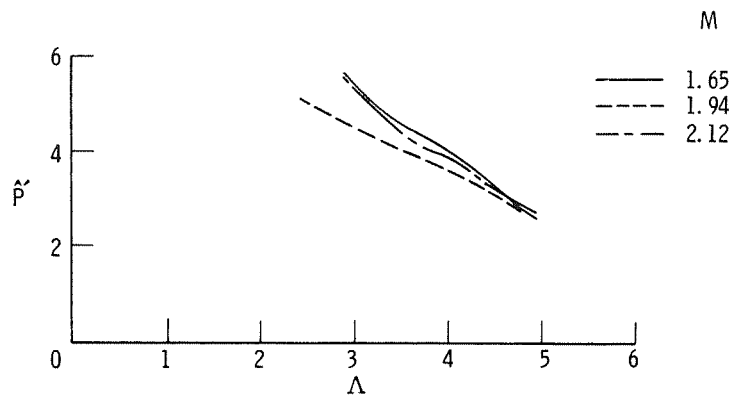
(b) M = 1.65 to 2.12.
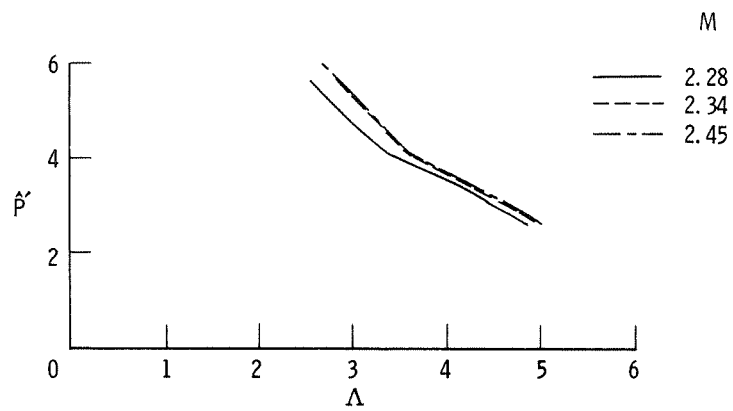
(c) M = 2.28 to 2.45.

Figure 9. Nondimensionalized power spectral density data obtained from the Photocon transducer at location 2.
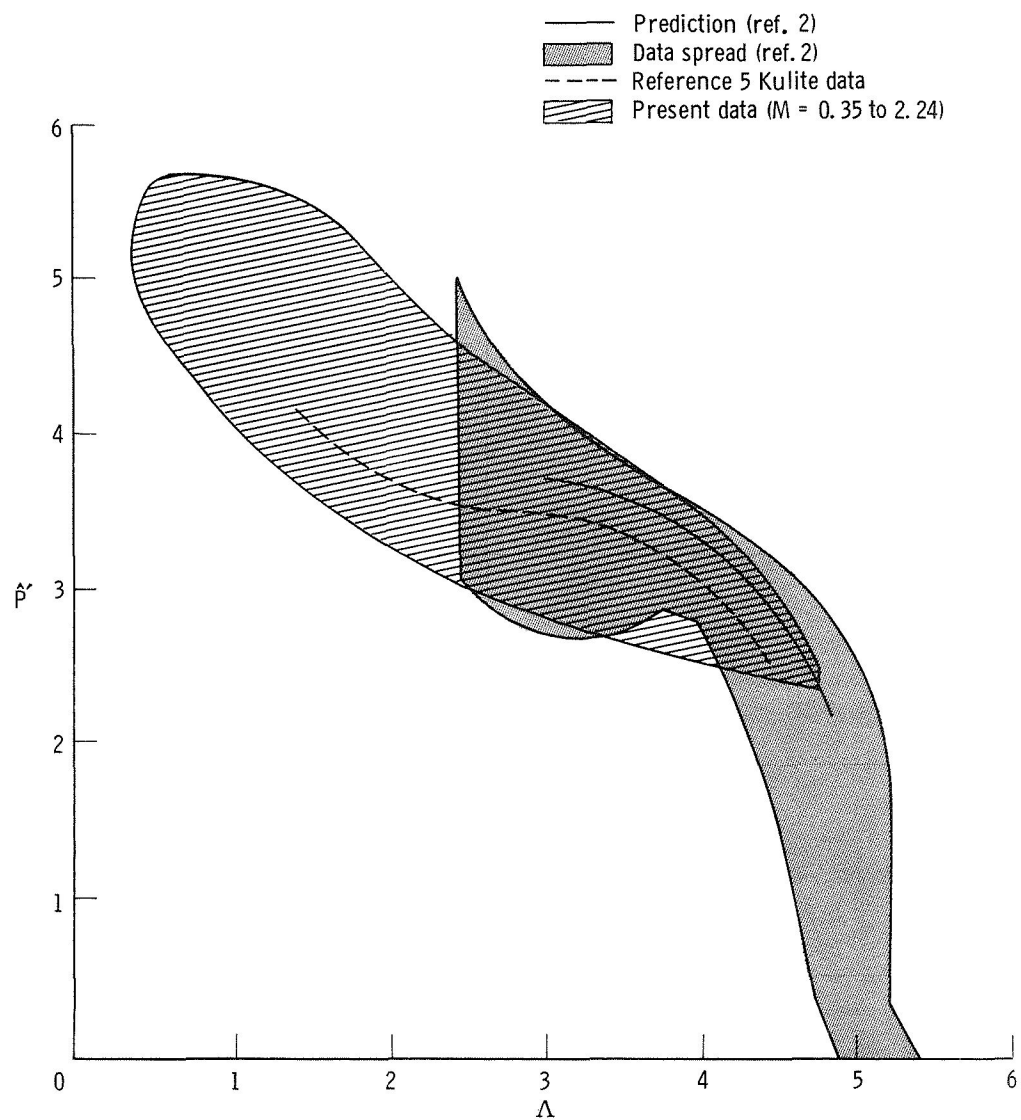
Figure 10. Comparison of nondimensionalized power spectral density data obtained from the Kulite transducers at location 1 with results from references 2 and 5.

24
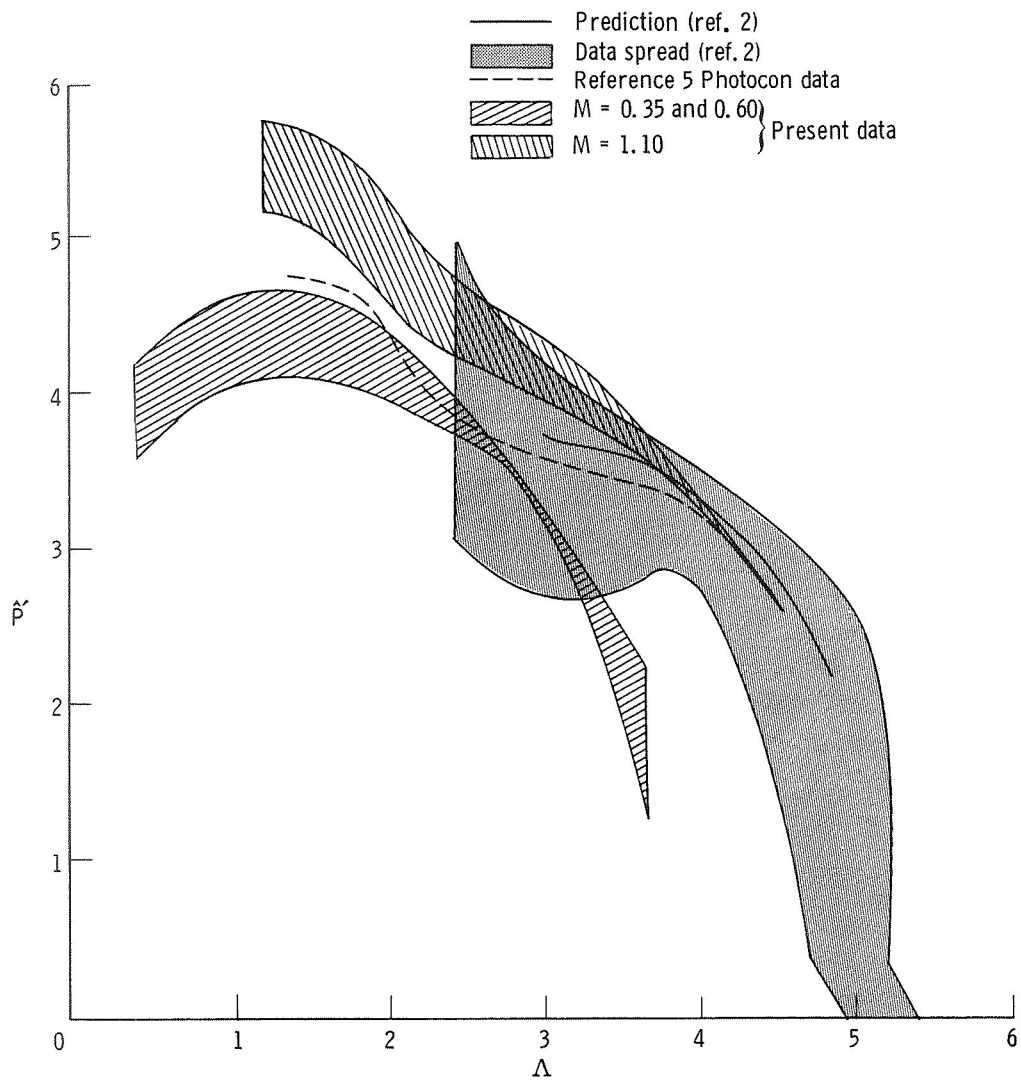
Figure 11. Comparison of nondimensionalized power spectral density data obtained from the Photocon transducers at location 1 with results from references 2 and 5.
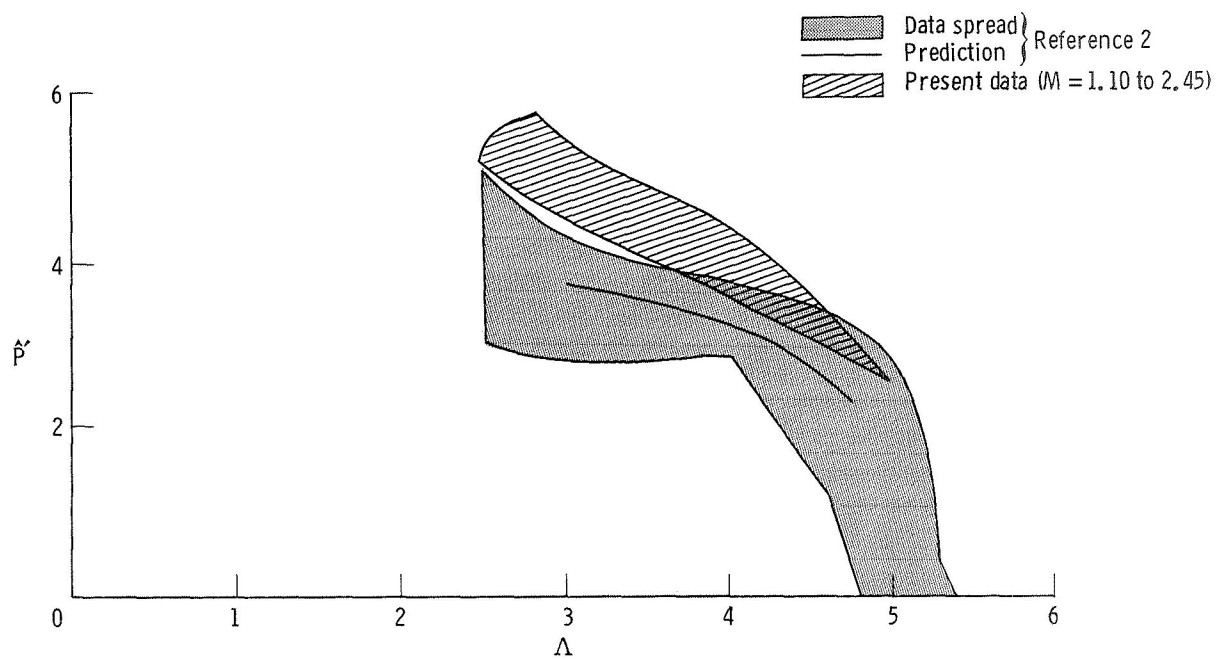
Figure 12. Comparison of nondimensionalized power spectral density data from location 2 for Mach numbers of 1.10, 1.65, 1.94, 2.12, 2.28, 2.34, and 2.45 with results from reference 2.
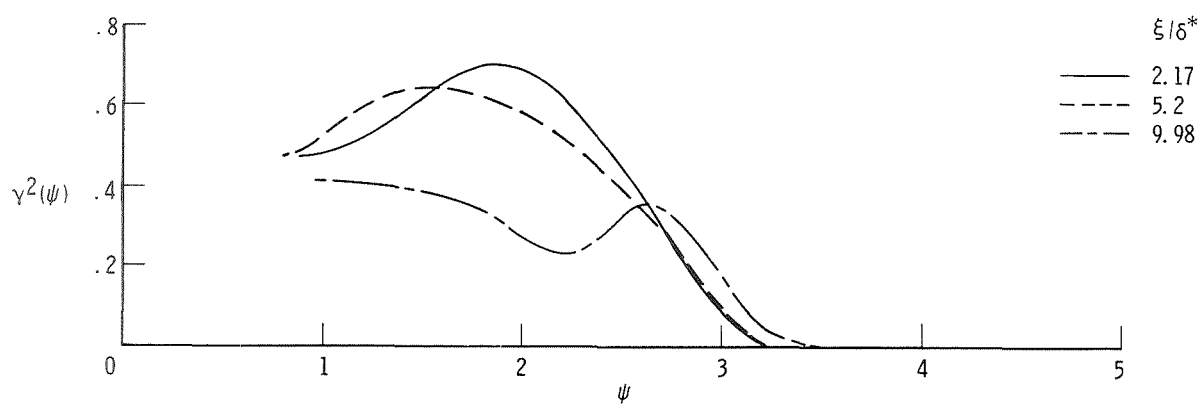
(a) M = 0.35.
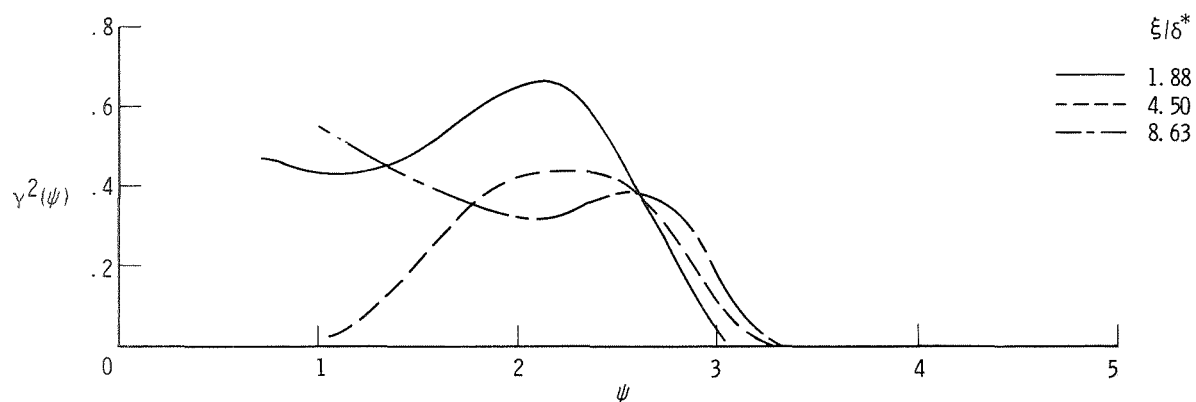
(b) M = 0.60.
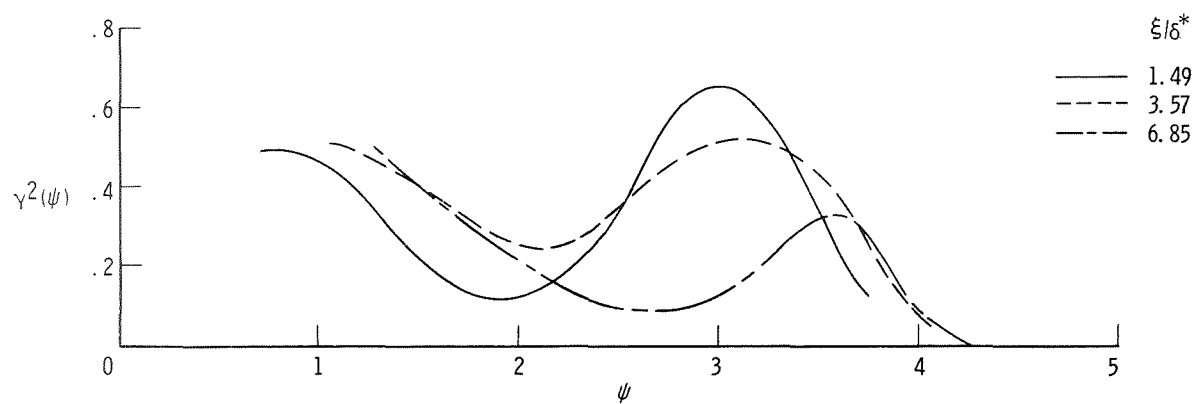
(c) M = 1.10.

Figure 13. Coherence function plots of surface-pressure fluctuations at location 1 for separation distances of 1.27, 3.05, and 5.86 cm (0.5, 1.2, and 2.3 in.).
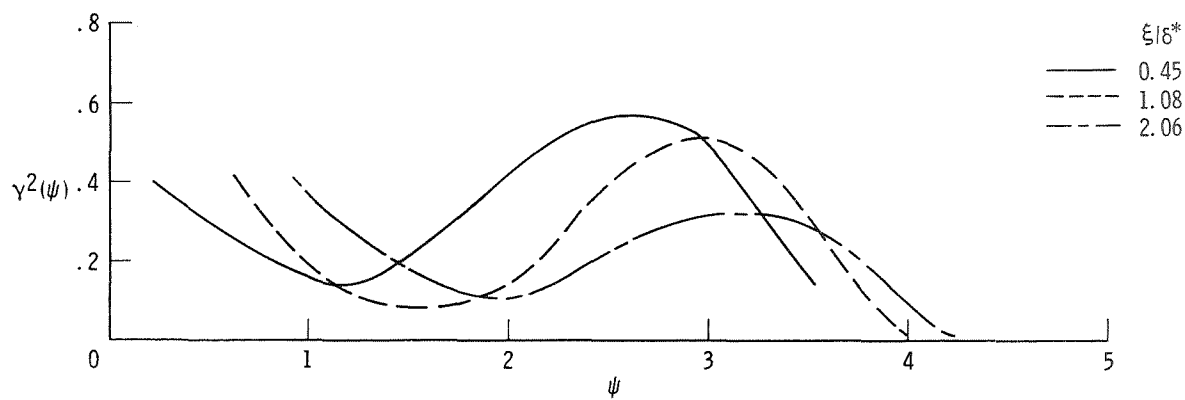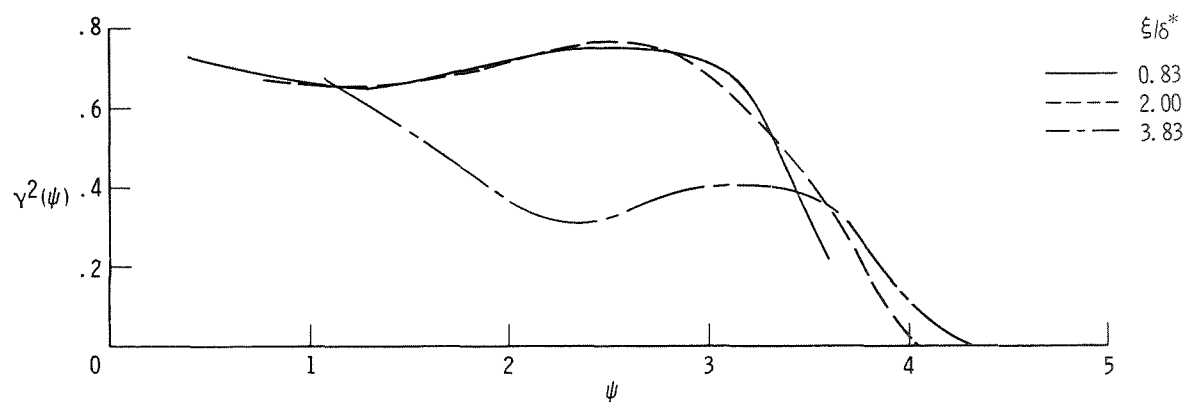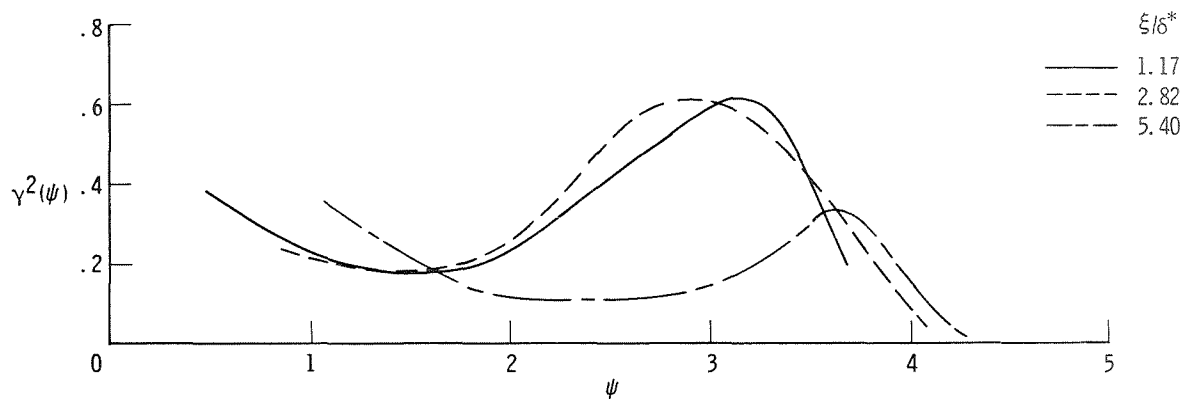
(d) M = 1.62.

(e) M = 1.92.

(f) M = 1.95.

Figure 13. Continued.
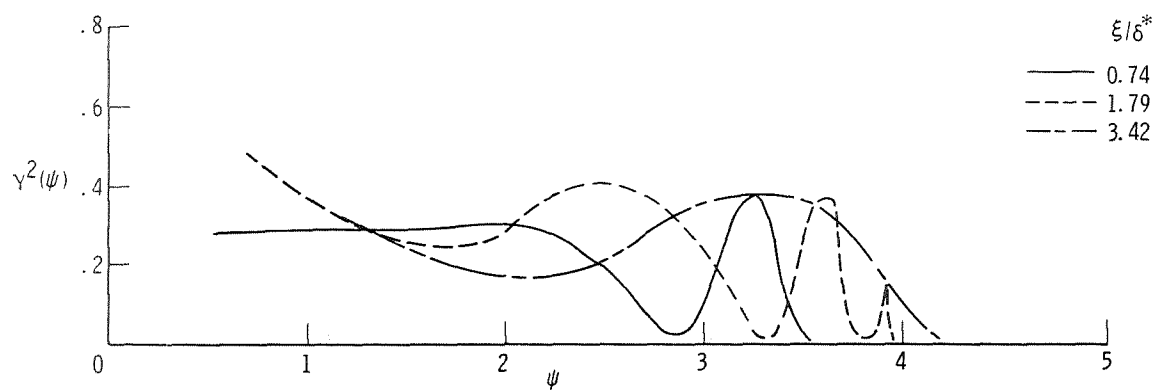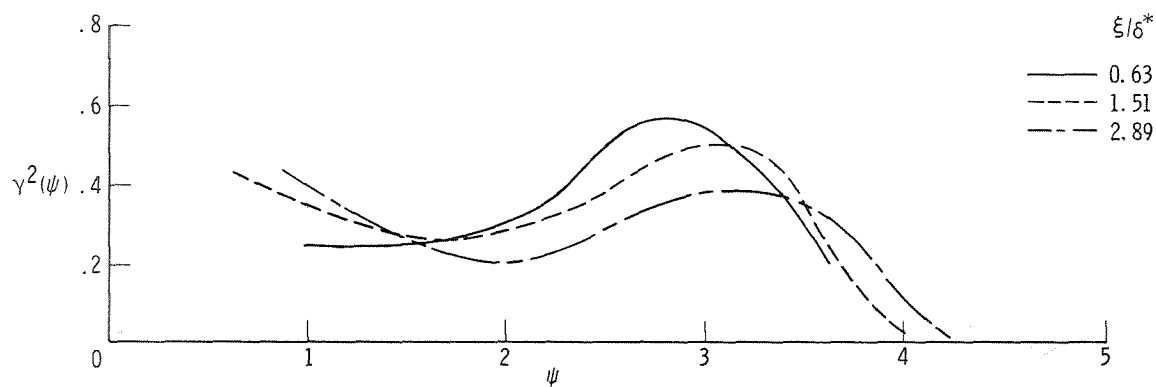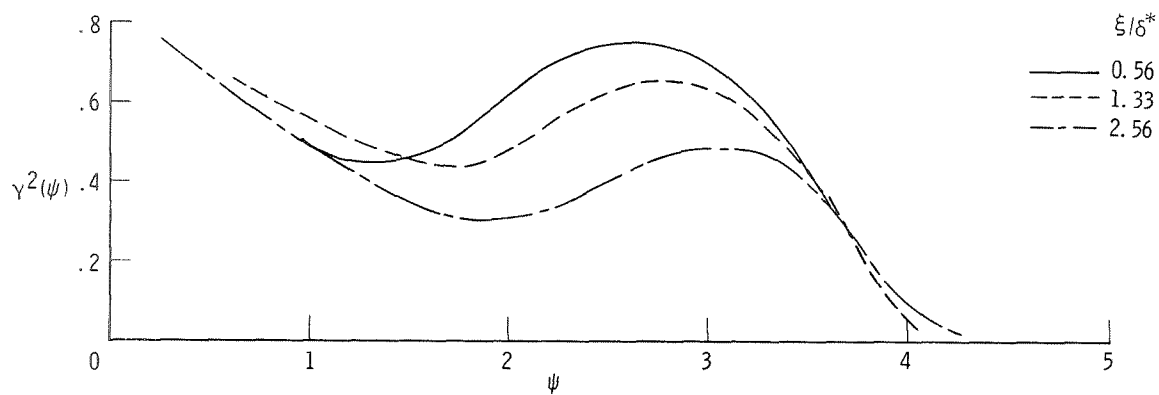
28

(g) M = 2.11.

(h) M = 2.21.

(i) M = 2.24.

Figure 13. Concluded.
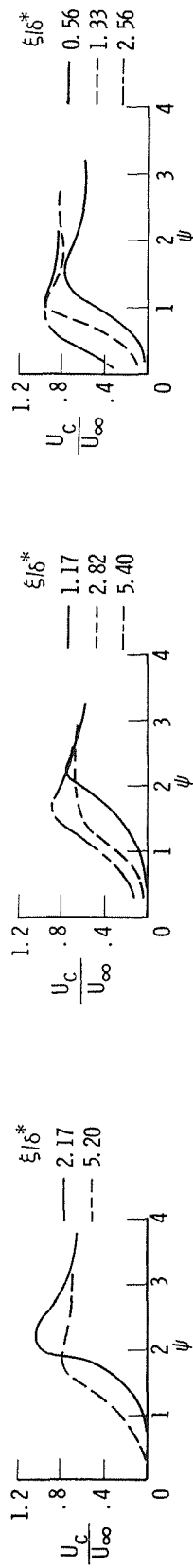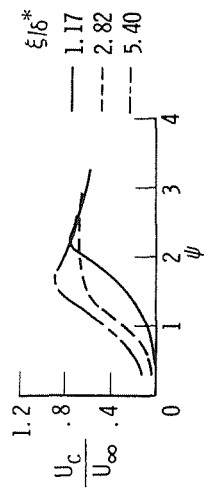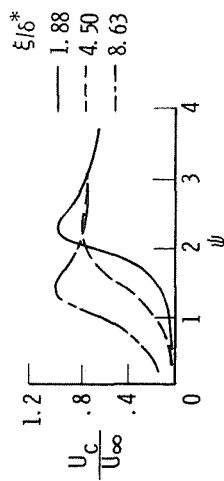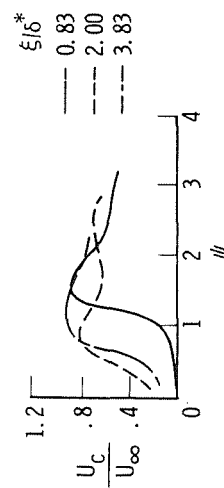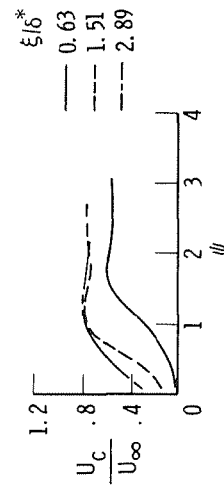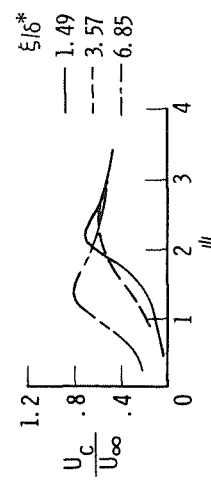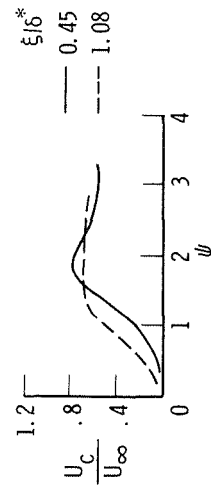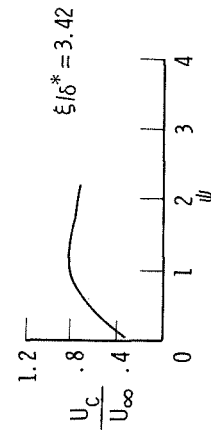
Figure 14. Narrow-band-convection velocity of the surface-pressure-fluctuation field at separation distances of 1.27, 3.05, and 5.86 cm (0.5, 1.2, and 2.3 in.).
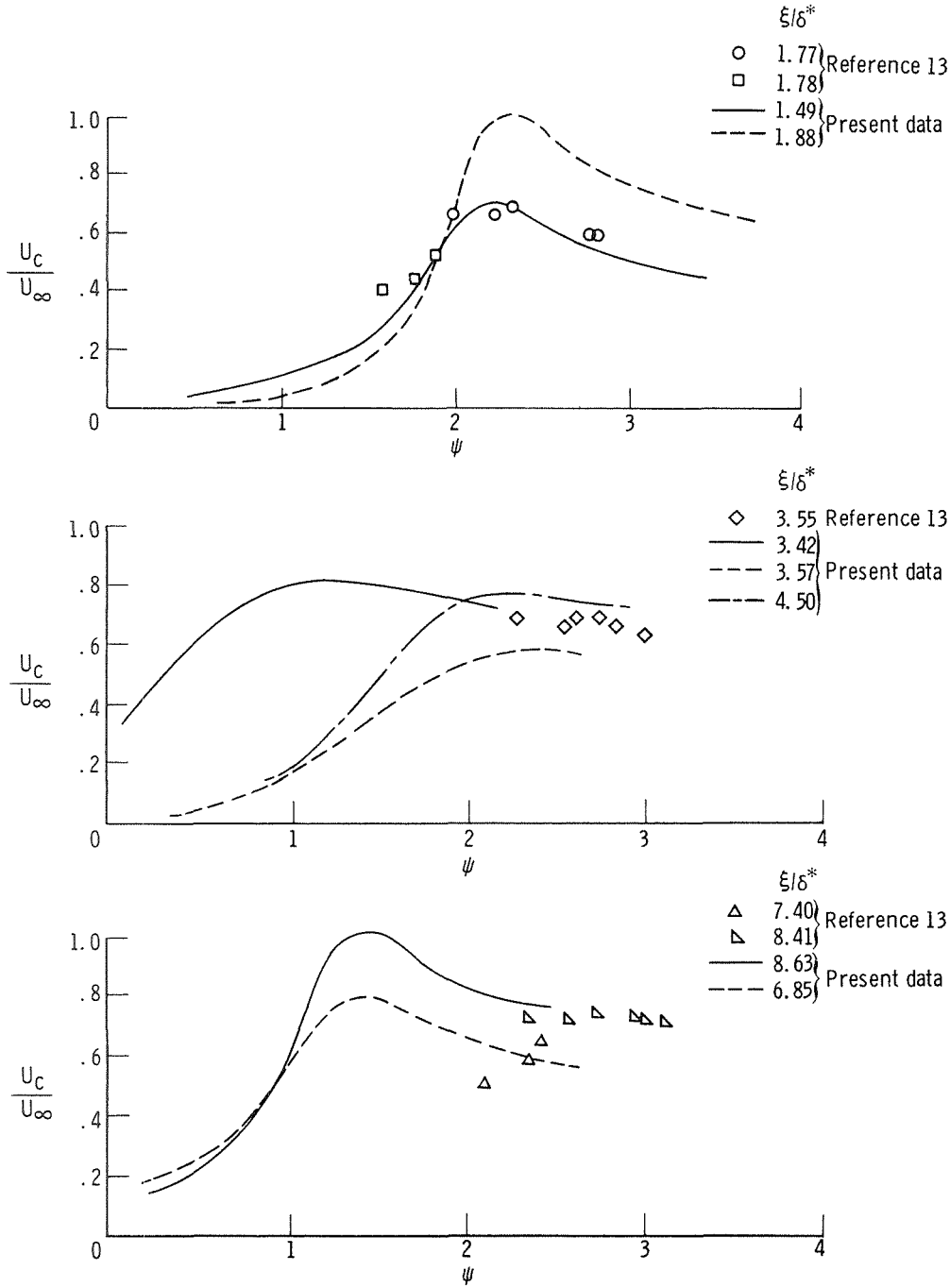
Figure 15. Comparison of surface-pressure-fluctuation narrow-band-convection-velocity data with similar data from reference 13.
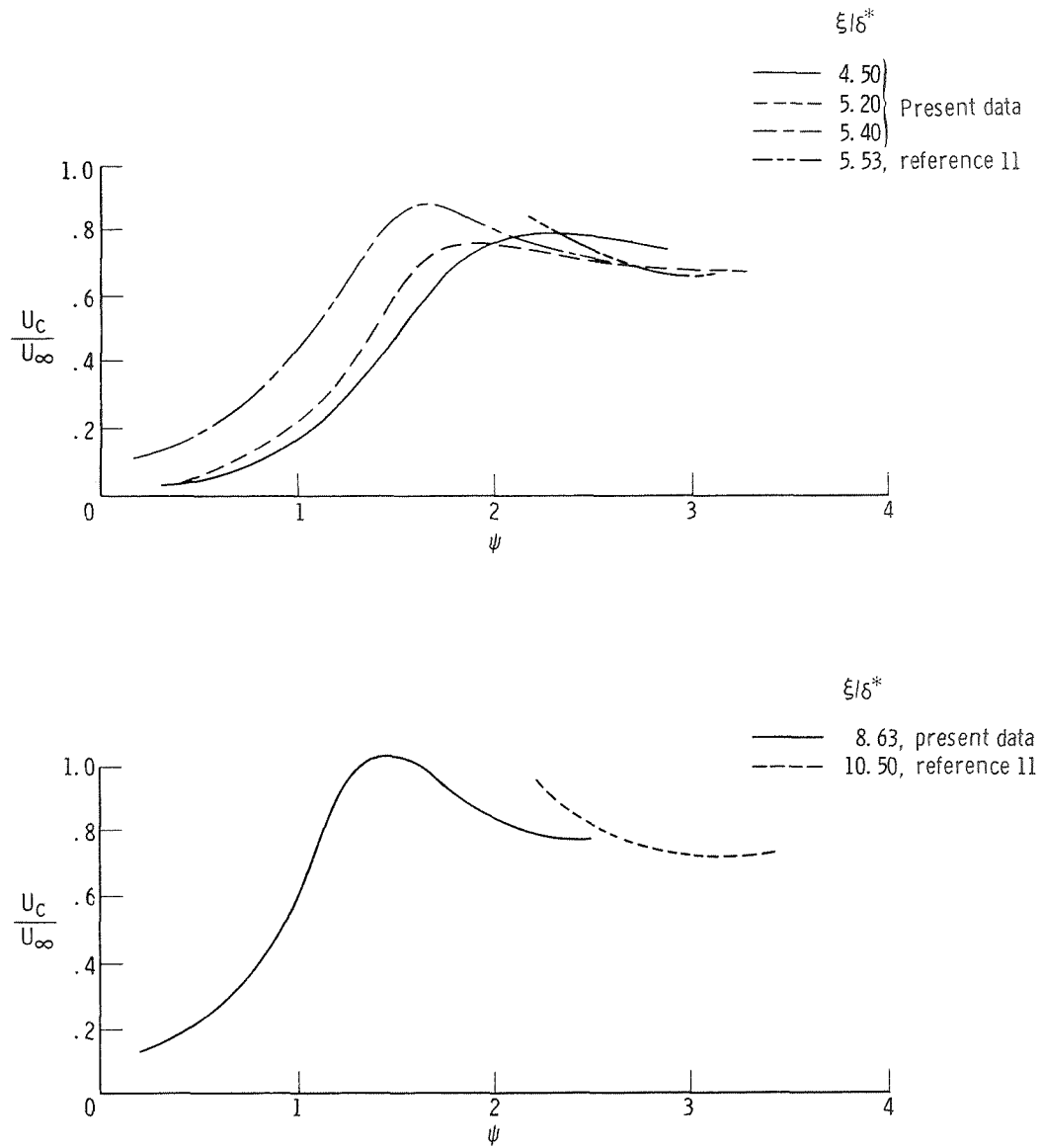
Figure 16. Comparison of surface-pressure-fluctuation narrow-band-convection-velocity data with similar data from reference 11.
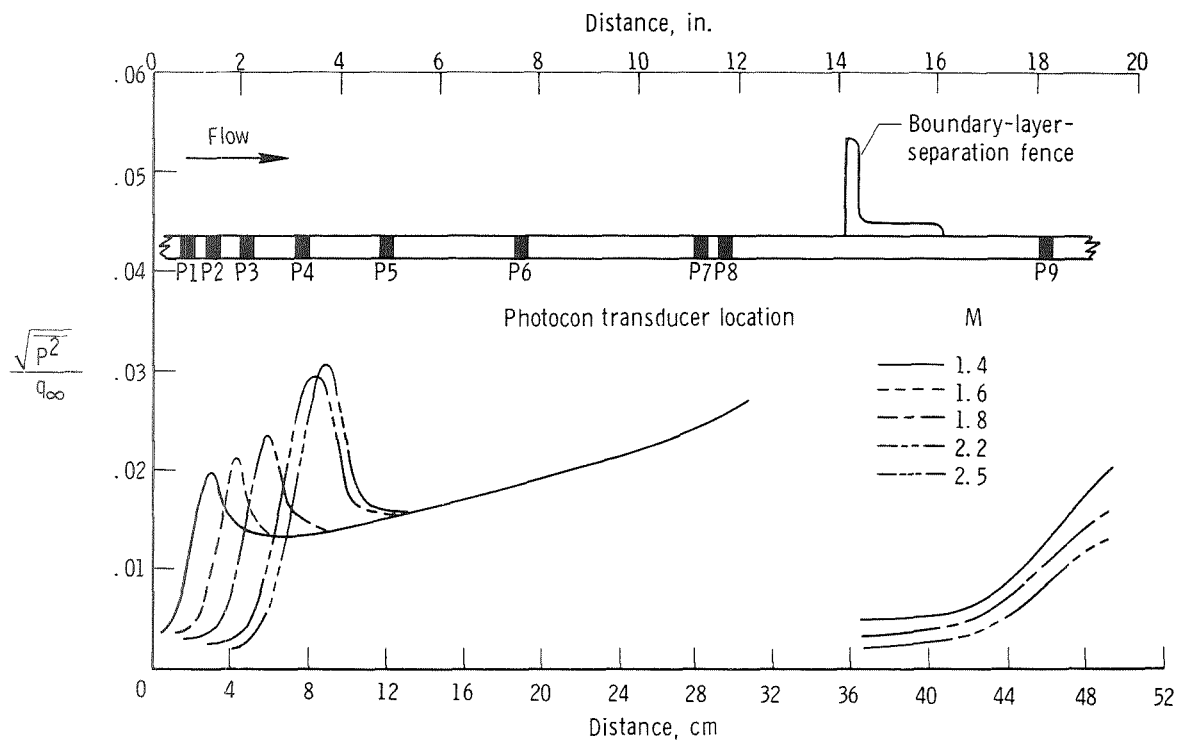
Figure 17. Variation of $\dfrac{\sqrt{P^2}}{q_\infty}$ along the surface showing the effect of a separated region of the surface flow on the surface-pressure-fluctuation field.

"The aeronautical and space activities of the United States shall be conducted so as to contribute . . . to the expansion of human knowledge of phenomena in the atmosphere and space. The Administration shall provide for the widest practicable and appropriate dissemination of information concerning its activities and the results thereof."

—NATIONAL AERONAUTICS AND SPACE ACT OF 1958

NASA SCIENTIFIC AND TECHNICAL PUBLICATIONS

TECHNICAL REPORTS: Scientific and technical information considered important, complete, and a lasting contribution to existing knowledge.

TECHNICAL NOTES: Information less broad in scope but nevertheless of importance as a contribution to existing knowledge.

TECHNICAL MEMORANDUMS: Information receiving limited distribution because of preliminary data, security classification, or other reasons. Also includes conference proceedings with either limited or unlimited distribution.

CONTRACTOR REPORTS: Scientific and technical information generated under a NASA contract or grant and considered an important contribution to existing knowledge.

TECHNICAL TRANSLATIONS: Information published in a foreign language considered to merit NASA distribution in English.

SPECIAL PUBLICATIONS: Information derived from or of value to NASA activities. Publications include final reports of major projects, monographs, data compilations, handbooks, sourcebooks, and special bibliographies.

TECHNOLOGY UTILIZATION PUBLICATIONS: Information on technology used by NASA that may be of particular interest in commercial and other non-aerospace applications. Publications include Tech Briefs, Technology Utilization Reports and Technology Surveys.

Details on the availability of these publications may be obtained from:

SCIENTIFIC AND TECHNICAL INFORMATION OFFICE

NATIONAL AERONAUTICS AND SPACE ADMINISTRATION

Washington, D.C. 20546